Applied Catalysis B: Environmental 110 (2011) 6–13

Contents lists available at ScienceDirect

Applied Catalysis B: Environmental

journal homepage: www.elsevier.com/locate/apcatb

Photodegradation of methyl orange and 2,3-butanedione on titanium-dioxide nanotube arrays efficiently synthesized on titanium coils

Vance Jaeger[a], Winn Wilson[b], Vaidyanathan (Ravi) Subramanian[a,*]

[a] Department of Chemical and Materials Engineering, University of Nevada, Reno, NV, USA
[b] Department of Civil and Environmental Engineering, University of Nevada, Reno, NV, USA

ARTICLE INFO

Article history:
Received 15 March 2011
Received in revised form 3 August 2011
Accepted 5 August 2011
Available online 1 September 2011

Keywords:
Photocatalysis
TiO_2 nanotubes
Methyl orange
Diacetyl vapors
Coil

ABSTRACT

This work presents the synthesis, characterization, and application of titanium dioxide nanotube arrays (T-NT) prepared on titanium coils by anodization. A comparison of the physical, photoelectrochemical, and photocatalytic properties of T-NT on coil, mesh, and foil architectures is reported. The application of T-NT on helical coils to UV–vis initiated photodegradation of pollutants in aqueous and gaseous phases is discussed. The T-NT on coil shows better photoactivity compared to T-NT on other geometries such as foil and mesh. A 30% increase in the photodegradation of methyl orange in the aqueous phase is noted with T-NT on coils compared to T-NT on mesh. T-NT on coils also demonstrate photodegradation of a model pollutant 2,3-butanedione (diacetyl) in the gaseous phase. The T-NT grown on the coil architecture offer several advantages such as significantly minimized dark spots, highly reduced recombination centers, as well as adjustable spacing and dimensions for tuning photo(electro)catalytic activity. This configuration can be useful in other non-photocatalytic applications as well.

1. Introduction

Titanium dioxide (TiO_2) has been widely studied as a photocatalyst for light-assisted remediation of environmentally toxic pollutants [1–8]. Irradiation of TiO_2 produces charged species that facilitate redox reactions at the photocatalyst surface [9–13] (and several other articles from different groups). Summarily, the process involves the formation of oxidative species, such as hydroxyl radials under irradiation, which break-down toxic pollutants to relatively benign and eco-friendly product(s) [14]. Eventually, the treated product may be discharged into the environment safely. Recently, ordered TiO_2 architecture has attracted significant attention as a photocatalyst. Of particular interest has been 1-D ordered titanium oxide nanotubes (T-NT) which have demonstrated interesting optical, catalytic, and electrocatalytic properties for various photo-related applications [15–18]. The synthesis of these T-NT is often carried out by the process of anodization of Ti followed by heat treatment to facilitate phase transformation. One of the main reasons this nanotube architecture has been promising compared to films made of granular TiO_2 is the improved separation of charged species realized with T-NT, attributable to highly reduced grain boundaries [19,20].

A review of recent literature shows that the anodization of titanium metal as a substrate results in the formation of T-NT with similar features, uniform dimensions, and high surface area [21–23]. The substrate transparency and geometry (such as foils, wires, and meshes) have been identified as key physical features that dramatically influence photoactivity of T-NT [24–27]. Earlier, we have demonstrated the benefits of producing nanotubes on a non-planar wire-type architecture [28]. Non-planar architecture offers the benefit of better light capture than a planar substrate, more efficient utilization of expensive titanium metal, and the possibility to eliminate the use of overlying expensive ad-atoms (atoms of elements that are added to assist a primary catalyst to enhance catalysis) for improving photoactivity. However, a significant challenge to the current preparation method for the T-NT is that a large volume of electrolyte is consumed during the anodization step, especially with non-planar geometries. Preparing nanotubes using small volume of electrolyte can be highly cost-effective.

Yet another relevant aspect of T-NT is its application as a photocatalyst in the degradation of environmental pollutants. An analysis of the literature in this area suggests that T-NT (i) effectively photodegrades a variety of pollutants [29,30], (ii) demonstrates better photodegradation kinetics compared to TiO_2 particulate films [19,20], and (iii) does not lose its photocatalytic activity after several cycles in operation [17]. However, the pollutants studied so far are limited to the aqueous phase only. An investigation of

* Corresponding author at: Chemical and Metallurgical Engineering Department, Room 310, LMR 474, Mail Stop 388, University of Nevada, Reno 89557, USA. Tel.: +1 775 784 4686; fax: +1 775 327 5059.
E-mail address: ravisv@unr.edu (V. (Ravi) Subramanian).

0926-3373/$ – see front matter © 2011 Elsevier B.V. All rights reserved.
doi:10.1016/j.apcatb.2011.08.005

the performance of T-NT in the photodegradation of gaseous phase pollutants has just started and is yet to be fully explored [31,32]. Particularly, the potential improvements realized by growing T-NT on non-planar Ti substrates in the gaseous phase photodegradation have not yet been examined.

We present three interesting findings in this work. Firstly, we demonstrate T-NT grown on a new non-planar helical coil-type architecture using the process of anodization and a comparison of the physical (length and diameter) and optical (absorbance) properties of these T-NT with T-NT prepared on foil and mesh. Secondly, the ability of the T-NT grown on these coils to perform photocatalytic degradation of representative pollutants in the aqueous as well as gaseous phases, the kinetics of the degradation process, and the superior performance of T-NT on coils with respect to T-NT on foils and mesh are discussed. Finally, a comparative analysis of TiO_2 nanoparticulate films and T-NT performance on different architectures and a discussion highlighting the benefits of T-NT formed on coils is also presented.

2. Experimental

2.1. Synthesis of T-NT on a coil architecture with highly reduced electrolyte volume and characterization of the T-NT

Titanium wire (99.7%) of O.D. 0.25 mm was obtained from Alfa Aesar and cut into lengths of 22 cm. The lower 20 cm of the wire was tightly and helically coiled around a 6 mm O.D. glass rod. The remaining 2 cm was bent into a crook that would allow easy attachment to an alligator clip. Two different configurations were used for the anodization. Configuration 1 was used for the plates and mesh. For this configuration a platinum flag electrode was placed in the solution 4 cm away from the bulk titanium. A volume of 300 ml of solution was used in a 500 ml beaker. This configuration is described in detail in earlier articles [33,34]. The samples were prepared using this method so that the photoactivity of T-NT on mesh and foil can be fairly compared with the newer method.

Configuration 2 was used strictly for the coils. In this method, the coils were placed around 1.5 mm I.D.–4 mm O.D. glass tube of 10 cm length. A 15 cm × 1 mm O.D. platinum wire was inserted into the inside of the glass tube, and 4 cm of the wire was allowed to hang out of the bottom of the tube. A slight bend was placed in the wire to keep the glass tube from slipping down the wire. The glass tube along with the titanium coil and the platinum wire were placed in a 25 ml graduated cylinder filled with 25 ml of the anodization solution. A schematic and a picture of the setup used for anodization of Ti with the coil configuration are shown in Supporting information S1. For both configurations, a bias of 20 V, 36 V, or 60 V was applied to the electrodes, and the anodization was carried out for different durations with the vessels in an ultrasonication bath. For anodization over 30 min, the water in the bath was changed at 30 min into the process to minimize heat-related deviations. After anodization, the coils were washed with DI water and allowed to dry overnight. All samples were annealed under a N_2 atmosphere at 550 °C for 2 h at a ramp rate of 4.5 °C/min.

2.2. Surface and photoelectrochemical characterization

The post-anodization and heat treated samples were characterized using scanning electron microscope (Hitachi S-4700 FE-SEM). Several sections of the coil samples were imaged in order to determine whether the proper and uniform structure of the nanotubes were present, as well as to measure the dimensions of the nanotubes. The nanotubes were further characterized for crystalline structure using XRD and indexed to JCPDS files. The analysis was performed by glancing angle X-ray diffraction equipment. The photoelectrochemical responses of the T-NT on different Ti configurations were measured using an Autolab potentiostat/galvanostat. A 1 M NaOH solution was used as the electrolyte in the photoelectrochemical measurements with Ag/AgCl as the reference and Pt wire as a counter electrode. For photoelectrocatalysis, external bias was varied between +0.0 V and +0.6 V vs. Ag/AgCl in steps of 0.1 V. For photovoltage measurements, intermittent irradiation was performed with the lights on for 50 s and lights off for 50 s. The scan voltage for chronoamperometric (I–t) studies was maintained at +0.0 V. Photocurrent densities determined from these measurements are normalized to the exposed geometrical area of the catalyst.

2.3. Photocatalytic degradation of aqueous and gaseous phase pollutants

2.3.1. Aqueous phase methyl orange (MO) photodegradation

An aqueous solution of 40 μM MO was prepared for testing the photocatalytic activity of the nanotubes. Photodegradation experiments were performed using 7 ml of the dye solution. The T-NTs were kept immersed in the cell with the MO. Continuous illumination of the T-NT immersed dye solution was performed for 30–120 min. A Newport® xenon light source (Part #366902) with an output of 500 W was used for photoillumination of methyl orange. The lamp source has an irradiation profile similar to natural solar radiation with light intensities extending from far UV to visible and infrared. A 0.5 M $CuSO_4$ solution was used to cut-off the far UV and reduce the intensity at the catalyst surface to 90 mW/cm^2. The details of the setup used here are based on an earlier work [35]. The distance between the light source and the sample was maintained constant at 3 cm to ensure that the light intensity at the catalysts surface is identical for all experiments (a luxmeter was used to confirm that the light intensities are the same). The photoreactor, geometrical area of illumination of the reactor (4×1 cm^2), and the volume of aqueous dye used (7 ml) in the photoreactor is the same for all experiments. The photocatalysis results are normalized to the illuminated geometrical area of the catalyst. Dye samples were withdrawn at regular intervals and then tested for UV–vis absorbance. The MO photodegradation was estimated from the decrease in the absorbance at 470 nm. The photocatalytic activities of T-NT on different geometries were tested in a similar manner. More details of the photocatalyst testing procedure including additional information on the apparatus are reported in an earlier work [17].

2.3.2. Gaseous phase diacetyl photodegradation

T-NT on Ti was placed in a quartz glass tubing of 20 cm length and an I.D. of 6 mm and an O.D. of 10 mm. The quartz tubes were incorporated into a flow system using polyethylene as the carrier hoses. The quartz tubes that carries the vapors were placed vertically alongside a cooling jacket containing a 450 W light source (Part #7825-34), powered by an Ace Glass® 450 W power supply. The light source emitted radiation stretching mainly between UV and visible light (40–48% UV, 40–48% visible, and balance IR). A 250 ml fluted Erlenmeyer flask containing approximately 3 g of 2,3-butanedione (diacetyl) was used as the source of pollutant. The diacetyl was carried by dry ambient air through the glass tubing containing the titanium coils. The volumetric flow rate of the carrier gas was determined and maintained constant by a flow gauge connected at the carrier gas entrance, and the motive for the gas flow was provided by a vacuum pump. After passing through the tubing, the gas was condensed using a dry ice and acetone trap. A mass balance was performed on the fluted Erlenmeyer flask and the water trap to determine conversion.

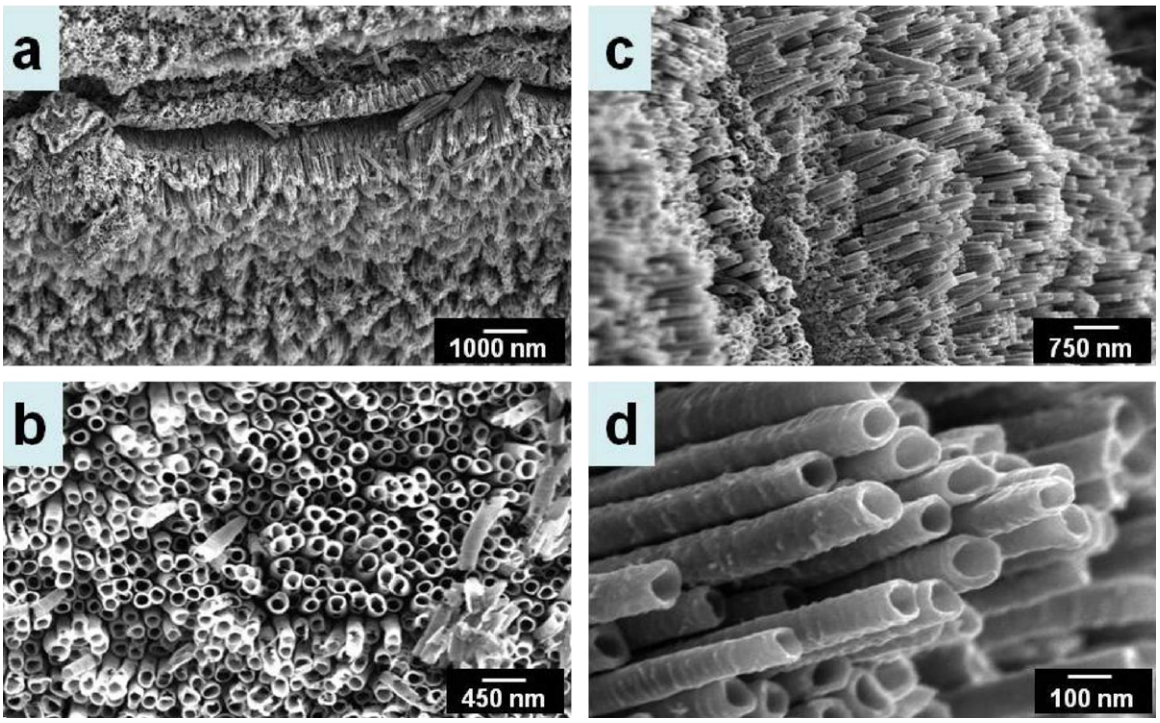

Fig. 1. Scanning electron microscope images of a representative set of T-NT prepared by anodization at 60 V for 60 min on (a and b) coils and (c and d) mesh. The different magnification image of the coil and mesh after anodization indicates details of the overall arrangement and the dimensions of the T-NT. The dimensions of the T-NT formed on coil and mesh obtained from the SEM images such as these are reported in Table 1.

3. Results

3.1. Comparison of the physical features of the nanotube on different supports

The T-NT formed on the Ti substrates were analyzed using SEM. They were examined at different orientations and found to be similar in all directions. The dimensions of the T-NT (length and diameter) grown on the Ti substrates were measured from the SEM images. The SEM images of the T-NT on the foil are not shown and readers are referred to an earlier report [17]. A representative series of SEM images at different magnifications of the T-NT formed on Ti coil and Ti mesh after anodization and annealing, is shown in Fig. 1. The T-NT formed on coils at 60 V for 60 min (Fig. 1a and b) and mesh under the same anodization conditions (Fig. 1c and d) are shown. These images show that the cylindrical and hollow nanotubes grow uniformly across the underlying Ti substrate. As reported in an earlier work [28], the curvature of the underlying Ti wire may induce cracks between the nanotubes as noted in Fig. 1. This aspect of T-NT growth is evident from Fig. 1a and c. A comparative analysis of the nanotube dimensions on different Ti configurations (foil, mesh, and coil) is also provided in Table 1. The effects of anodization voltage and duration are also compared in this table. In general it is noted that, as the voltage and/or the anodization time increases, the length and diameter of the nanotube increases for all the Ti configurations.

We take a closer look at the T-NT grown on the non-planar mesh and coil configurations since they are prepared with two different electrolyte volumes. It is noted that, with both these configurations, the variations in the nanotube dimensions at any given voltage are insignificant. This observation highlights a few interesting features of the anodization process developed here. A key aspect is that one can achieve these almost identical dimensions (300–800 nm length and 60–100 nm diameter) in spite of reducing the electrolyte volume to a fraction (from 300 ml to 25 ml). Further, the time required for producing nanotubes of any desired dimension remains in the same range (30–60 min) though the volume of the solution is considerably reduced.

Another crucial parameter worth taking a note during the anodization process is the current measured during T-NT formation [36]. It is well known that the nanotube formation occurs through dissolution and re-precipitation of Ti ions and accompanied with an oxidative current during anodization. We observe (i) a finite and stable current during anodization of the Ti coil and (ii) an increase in its magnitude with anodization voltage. It indicates that the mechanism as well as the extent of T-NT growth on the coils is similar to the process noted with foil [36]. This observation suggests that the formation and growth mechanism of T-NT on Ti is not affected by the significant reduction in the volume of the electrolyte.

Thus the beneficial aspects of the modified anodization method, include (i) preparing T-NT on non-planar geometries such as a coil, (ii) synthesis of T-NT with no change in dimensions, and (iii) an approach that is less expensive, more effective, and just as timely as previously reported methods.

3.2. Surface, optical, and photoelectrochemical properties of the anodized films

3.2.1. Surface properties

Fig. 2 shows the XRD profile of the anodized samples prepared with the reduced volume of electrolyte. Distinct peaks from the samples noted at several 2θ values as marked in the figure indicate that the material is crystalline. The peaks can be indexed to the JCPDS files [44-1294-Ti, 21-1272-Anatase TiO_2]. The identity of these peaks indicates that the material is anatase phase TiO_2. The formation of the predominantly anatase phase may be attributed to the heat treatment under nitrogen [48]. The XRD was compared to a sample prepared using the regular volume of electrolytes. The peaks match with the ones shown in the XRD indicating that both methods of T-NT synthesis produce similar samples. It is important

Table 1
A comparison of the physical features (length and diameter in nm) of T-NT formed on Ti foil, mesh, and coil at different anodization voltages and time. Note that the reduction in electrolyte volume from 300 ml to 25 ml does not alter the physical features of the T-NT on coil.

Voltage (V)	Time (min)	Foil[a]		Mesh[a]		Coil[b]	
		Length	Diameter	Length	Diameter	Length	Diameter
20	30	280	50–60	280	50–60	300	60–70
20	45	360	50–60	430	60–70	450	55–65
20	60	470	60–70	650	65–75	600	65–70
36	60	560	85	600–750	80–90	600–700	90–100
60	60	600–700	105	–800	85–100	>800	100–110

[a] Configuration 1.
[b] Configuration 2.

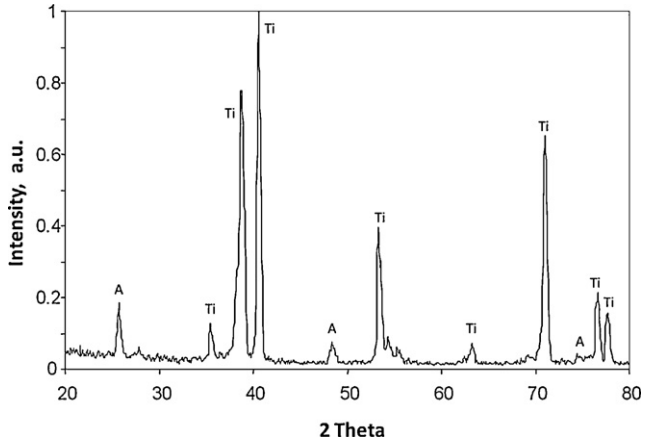

Fig. 2. X-ray diffraction pattern of the T-NT on coil prepared by anodization in 25 ml of electrolyte followed by heat treatment at 550 °C for 2 h. Peaks corresponding to crystalline anatase phase of T-NT (indicated by A), and underlying titanium (indicated by Ti) are marked.

to mention here that anodization of Ti using various other electrolytes has also been reported. Based on these results, it is reasonable to expect that the crystalline properties of the anodized samples will remain unaltered should volume for other reported electrolyte compositions be reduced as well.

3.2.2. Optical properties

Absorbance measurements provide information about the photoactive region of the catalyst. Fig. 3 shows the optical absorbance spectra of the anodized and heat treated sample. A T-NT on foil is also shown as a comparison. The spectra were obtained from the diffuse reflectance measurements by performing Kubelkamank transformations. In the case of T-NT on coils, the sample was gently compacted to obtain the spectra. T-NT produced by anodization of Ti coils exhibits absorbance features similar to T-NT on foil. This shows that the T-NT is mainly active in the UV region.

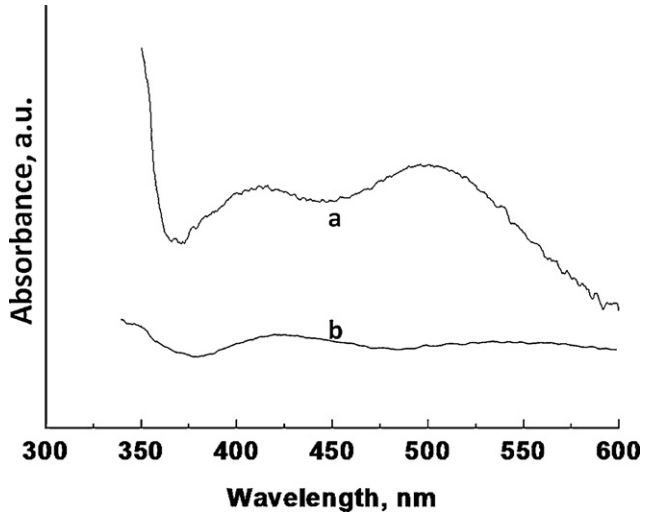

Fig. 3. The absorbance spectra of (a) T-NT on foil prepared using 300 ml of electrolyte and (b) T-NT on coil prepared using 25 ml of electrolyte in the anodization process followed by heat treatment at 550 °C for 2 h is shown in the figure.

The surface and optical studies confirm that reduction in volume does not change the characteristics of the product formed after anodization and heat treatment.

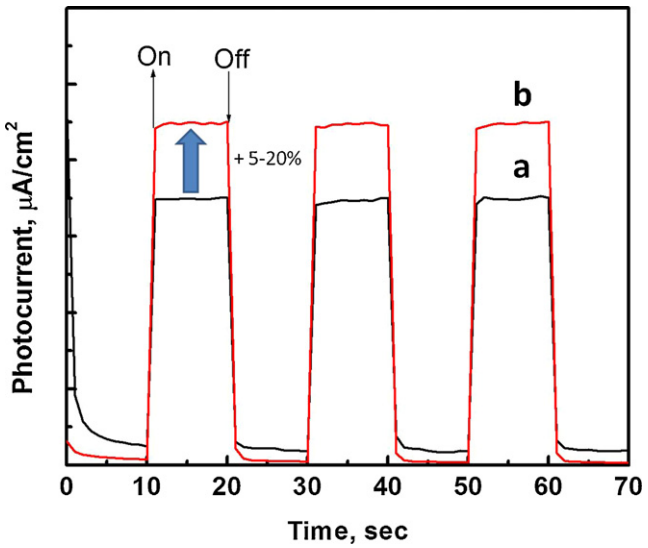

Fig. 4. The photocurrent responses of T-NT prepared on (a) Ti mesh and (b) Ti coil normalized to exposed geometrical surface areas is shown. The measurements were performed in 1.0 M NaOH solution as electrolyte using Pt as the counter electrode. A 5–20% improvement in the photocurrent response is noted depending on anodization conditions (voltage and duration) used to prepare the T-NT. Specific values of photocurrent are given in Table 2.

3.2.3. Electrochemical properties

Photoelectrochemical measurements provide information about the photogenerated charge separation and transport in a photocatalyst [37]. These responses for T-NT prepared on mesh and coil are shown in Fig. 4. A comparative analysis of the photocurrent values obtained from T-NT on coil and mesh indicates that the photocurrent is higher by 5–20% for the coil compared to the mesh as shown in Table 2. It is to be noted that the data reported in Table 2 and Fig. 4 are normalized to exposed geometrical area of the photocatalysts used in that experiment. This can be attributed to the varying dimensions of the T-NT formed under different anodization voltage and time (Table 1). Further, the changes in the baseline dark current can be attributed to the nature of equilibrium existing at the electrode–electrolyte interface and the discharge rate of photogenerated charges once the photo-illumination is

Table 2
A table comparing the photocurrent values obtained using T-NT formed on planar (foil) and non-planar (mesh and coil) geometries under different anodization conditions. The photocurrent values normalized to exposed geometrical area are noted to be higher by 5–20% using T-NT formed on coils compared to T-NT formed on any other substrates.

Voltage (V)	Time (min)	Foil	Mesh	Coil
		I_{Ph} (μA/cm^2)	I_{Ph} (μA/cm^2)	I_{Ph} (μA/cm^2)
20	30	71	95	102
20	45	75	100	121
20	60	77	110	115
36	60	83	105	130
60	60	91	100	121

switched off. In most cases, an instantaneous change in the photocurrent is noted as soon as the sample is illuminated, indicating prompt photo response. The photovoltage characteristic is shown in Supporting information S2. Similar trends in the observation can also be made with *V–t* measurements. The results of the on–off cycles indicates that the *I–t* responses of the anodized films on the coil and mesh geometries are reproducible.

3.3. Photocatalytic degradation studies in aqueous and gaseous phases using T-NT on coils

3.3.1. Aqueous phase photodegradation of methyl orange (MO)

The byproducts of coloring materials such as azo-dyes used in textile industries are discharged into water bodies or stored in landfills after concentrating with high surface area absorbers such as activated carbon [38]. These dyes are often toxic and if the water is left untreated they can cause environmental and health damage [39]. MO is a representative dye of the azo-dye family which is commonly linked to aquatic pollution and health-related problems such as cancer [40,41]. Its photo responses are similar to other dyes from the same family of compounds. Therefore, several research articles have examined and discussed the photodegradation of this dye using TiO_2 [42–44] and its composites [45,46]. For the aforementioned reasons as well as for comparing with our earlier work, MO was chosen as the compound of interest in this study. It is known that the photodegradation mechanism of MO on TiO_2 follows a pathway that involves formation of hydroxylated and non-hydroxylated species as intermediates before leading to benign products [47]. However, the rates of photodegradation vastly vary depending upon the type of photocatalyst used.

The liquid phase photodegradation of MO using T-NT on coil and mesh is discussed below. The fractional conversion of the dye following continuous illumination was examined from the absorbance data (Supporting information S3) using the expression[48]:

$$X_{MO} = \frac{[MO]_0 - [MO]_t}{[MO]_0} \quad (1)$$

where $[MO]_0$ and $[MO]_t$ = MO concentration at $t = 0$ and after different time intervals t. The performances of the T-NT on foil, mesh, and coil are compared in Fig. 5. The conversion of MO is normalized with respect to the exposed geometrical surface area of the T-NT grown on Ti mesh and coil. It can be seen that the photodegradation of the dye is highest at ~50% with T-NT on coil compared to the T-NT on other geometries. The T-NT on coil shows a 30% improvement in the degradation of MO compared to T-NT on mesh. The mesh demonstrates better photocatalytic degradation compared to the foil which shows ~20% conversion of the dye. The experiments were repeated and the data is found to be within a margin of error of ±5%. Baseline blank experiments without T-NT did not show any measurable photodegradation of MO. This was concluded after noting that there was no decrease in the peak absorbance at 470 nm after illumination of MO solution for 2 h.

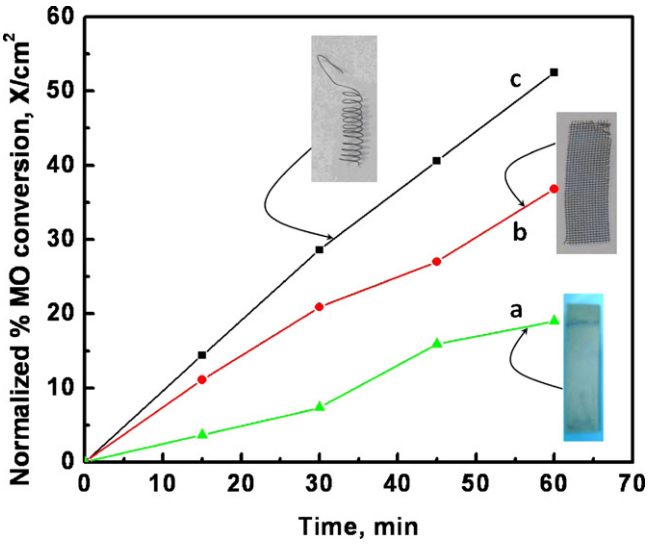

Fig. 5. A comparison of the percent conversion of MO using T-NT formed on (a) Ti foil, (b) Ti mesh, and (c) Ti coil normalized to illuminated surface area. A 40 (M solution of MO was continuously illuminated with UV–vis light in the presence of the photocatalyst for 60 min. Samples were drawn intermittently and analyzed using absorbance spectroscopy to examine the extent of MO degradation.

Further, it has previously been reported that the photodegradation rates of pollutants such as dyes can be significantly accelerated by the application of an external bias on film-based photocatalysts [17]. We have examined the effects of bias on MO photodegradation with both coil and mesh architectures. The photodegradation of MO was performed at various bias ranging between +0.1 and +0.6 V vs. Ag/AgCl. The initial conversion data, normalized to the illuminated area of the nanotubes obtained after 15 min of continuous illumination, is reported in Table 3. It can be noted that the normalized conversion of MO with the coil geometry is higher than the conversion observed with mesh.

The kinetic parameters of a photodegradation process can be determined using power law model. This model has the general form [49]:

$$-r = -\frac{d[MO]}{dt} = k[MO]^n \quad (2)$$

where $-r$ = rate of the reaction, k = rate constant, and n = order of the reaction. This form of expression is often used in estimating the rate constant and order of reaction for dye photodegradation on TiO_2. The data obtained from the external bias experiments were analyzed using the linearized form of Eq. (2) assuming a pseudo first order process. The rate constant values are reported in Table 4. The rate constant is in general noted to be higher with coil than the mesh. Thus, the photodegradation for MO is higher on T-NT prepared on coils compared to T-NT on mesh.

Table 3
The normalized percent photodegradation of MO obtained at different external bias voltage after 15 min of continuous illumination using a 3-electrode configuration with T-NT formed on Ti coils as the working electrode and a Pt wire as the counter electrode. The T-NT was prepared on mesh and coil using NH_4F in ethylene glycol as electrolyte at an anodization voltage of 60 V for 30 min. All the bias experiments were performed with respect to Ag/AgCl as the reference electrode.

Bias*1→Substrate*2↓	+0.0 V	+0.1 V	+0.2 V	+0.4 V	+0.6 V
T-NT/mesh	4.5	6.4	7.6	8.4	12.1
T-NT/coil	6.2	10.2	10.4	11.5	15.4

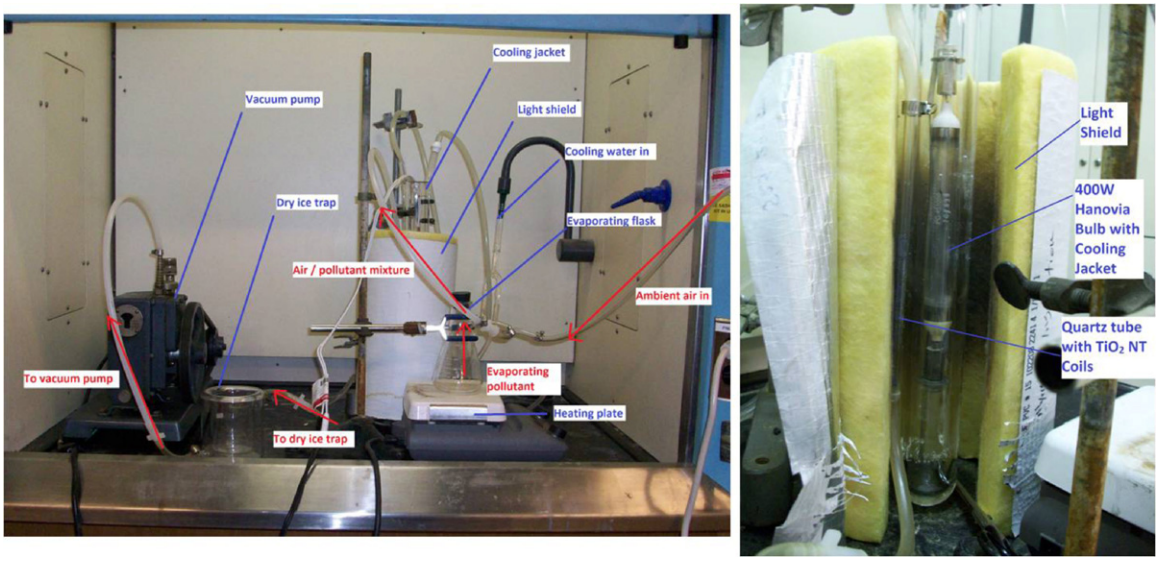

Fig. 6. The photograph of the setup assembled to perform the photocatalytic degradation of acetyl vapors. An inert gas was used as a carrier for acetyl vapors by bubbling in an acetyl solution and passed through the reactor. A view of the reactor (after removing the UV protection screen) with the light source is shown on the right hand side.

Table 4
The values of the rate constant obtained by applying the first order power law model to the fractional conversion data obtained from MO photoconversion. Data shown in Table 3 was used as input for estimating the parameters with the power law model. All the bias experiments were performed with respect to Ag/AgCl as the reference electrode.

Bias*1 →Substrate*2↓	+0.0 V	+0.1 V	+0.2 V	+0.4 V	+0.6 V
T-NT/mesh	0.0016	0.0022	0.0027	0.003	0.0043
T-NT/coil	0.0022	0.0035	0.0037	0.004	0.0054

3.3.2. Gaseous phase photodegradation of diacetyl vapors

The objective here was to examine the application of the T-NT on coils for photodegradation of diacetyl in the vapor phase. Recent studies have linked exposure to diacetyl chemical vapors to a medical condition called bronchiolitis obliterans in which the lungs of the victim are irreversibly damaged [50,51]. Further, strong odor from the chemical can be a significant inconvenience. Therefore the application of photodegradation methods to combat the odor has been studied [52]. While no current regulations exist in the United States that would limit worker exposure to the chemical, occupational safety and health administration (OSHA) has considered setting such limits.

Fig. 6 shows the pictures of the entire setup and cross section view of the reactor area. Ambient air flows in from the right where it is mixed with the evaporating pollutant. This mixture is moved through the reactor (details of flow shown in Fig. 6). The gas is passed through a quartz tube reactor containing varying number of coils while it is illuminated by the bulb. Once the gas passes out of the reactor, it is frozen in a dry ice trap and the ambient air is allowed to flow forward and vented through an exhaust.

Photodegradation experiments were run with the 20 cm coils anodized at 60 V for 30 min in the 25 ml of anodization electrolyte. Several coils were used since the gaseous phase residence times are significantly shorter than aqueous phase systems and it is harder to control gas flow than in aqueous phase systems. Multiple coils allowed for mimicking the effect of higher area on the conversion of the gaseous phase pollutant. The pollutant and ambient air were pumped into the photocatalytic chamber at 4.7 (10 scfh). Fig. 7 shows the conversion of the pollutant as a function of number of coils placed in series. Two sets of experiments were performed and the plot indicates similar magnitudes of conversion with different numbers of coils. It is to be noted that diacetyl can be degraded in the absence of the coil and hence the fractional conversion in the absence of the photocatalyst is also reported in Fig. 7. The data suggests that after an offset of the photocatalyst – free conversion (shown by dotted baseline), a conversion of 45% can be achieved with 24 coils placed in series one after the other.

4. Discussions

4.1. Unique features of the T-NT grown on a coil architecture

The photoelectrochemical and photocatalysis experiments demonstrate that T-NTs grown on the coil architecture are not only photoactive but also capable of performing photodegradation effectively compared to T-NT on mesh or foil. Herein, important benefits of growing T-NT on a coil architecture compared to other non-planar geometries are presented. These include ability to (i) maximize catalyst–light interaction by reducing 'dark

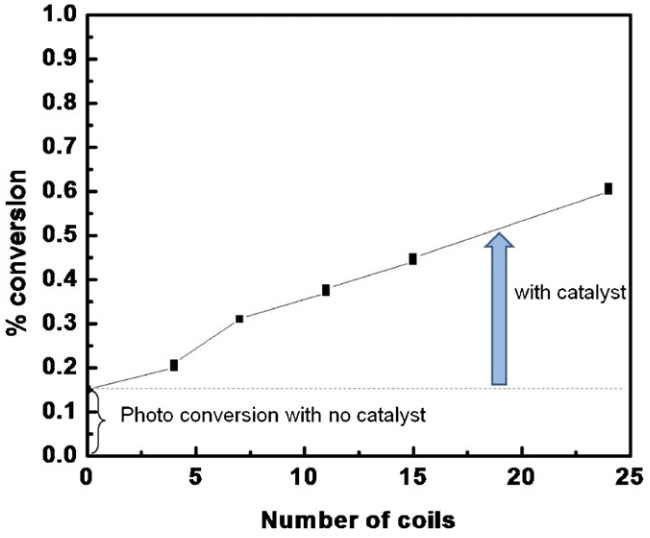

Fig. 7. The photocatalytic degradation of diacetyl vapors performed using T-NT prepared on Ti coil by anodization in 25 ml of electrolyte. A one-pass tubular reactor with the option to place several tens of coils in series was used to study the effect of increase in the surface area on the photodegradation of diacetyl vapors.

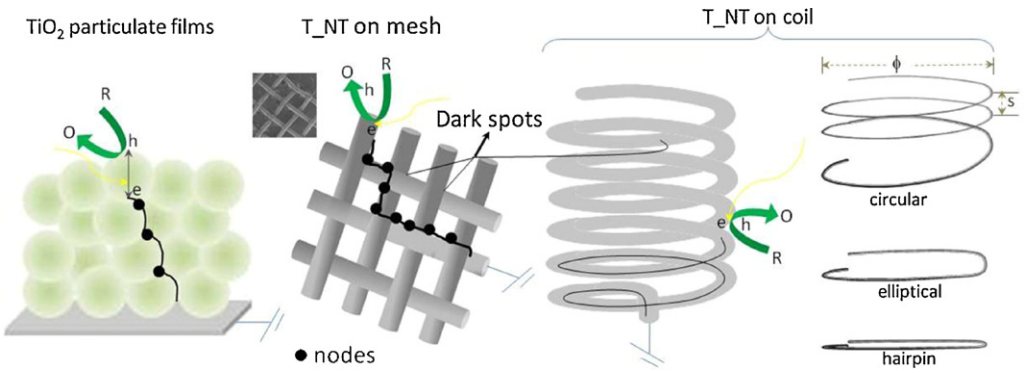

Fig. 8. TiO_2 in particulate film, mesh, and coil configuration is shown along with the pathway the photogenerated electron–hole traverse after illumination. Dark spots or nodes function as recombination centers in a mesh architecture just as grain boundaries do in TiO_2 particulate films. The absence of such nodes in a coil architecture favors improved e^-–h^+ separation and transforms into better photocatalytic activity.

spots' or nodes, (ii) improve electron–hole separation (favorable for enhancing photoelectrocatalysis), and (iii) adjust the spacing between successive coil turns for efficient catalyst utilization and tunable photocatalytic conversion. These aspects are briefly discussed below and elaborated by the scheme shown in Fig. 8.

4.2. Significantly low dark spots or nodes

In a mesh, several titanium wires are assembled together in a crisscross arrangement. Such an overlapping between wires causes periodic spots where no light can impinge on the underlying wire. This can be observed at alternate locations between successive wires and is referred to here as dark spots or 'nodes'. From a photocatalysis standpoint, the nodes are non-participating areas of the mesh since light cannot reach these spots. A significant reduction in the mesh size increases the number of such nodes per unit illuminated area. In fact, coils have less than one-tenth the dark area of the mesh (0.5% for coil vs. over 6% for mesh) as calculated by the area of the shadow that the Ti substrate casts upon itself). In turn, this reduces the photocatalytic efficiency. Such overlapping areas are significantly curtailed in a coil configuration. As a result, the catalyst–light interaction is maximized promoting greater photocatalytic activity. The photocatalytic data of Fig. 5 is evidence of this benefit.

4.3. Highly reduced recombination centers

Often in meshes, the nodes are not welded joints. This leads to the formation of nanotubes at the nodes during the anodization process as the electrolytes can diffuse into these inner spaces. The T-NT present at these nodes function as a resistor to electron transport. Several nodes will lead to a significant contact resistance that can function as recombination centers for electrons and holes. The contact resistance is akin to interparticulate grain boundaries in films prepared from colloidal nanoparticles [53]. Due to the constant resistance, the electron transport in a mesh can be reduced. Alternately, there is negligible contact resistance in a coil configuration. Performing a resistance measurement of anodized coil and mesh shows that a mesh has a resistance of 17.5 kΩ while a coil has 10.5 kΩ respectively. This observation suggests that the contacts at the nodes of a mesh are not completely flush since the T-NT cylinders form barrier layers that impede electron flow. In fact, the lower values of photocurrent and photovoltage, as determined from the photoelectrochemical measurements for the mesh compared to the coil (Fig. 4 and Table 2) also provides the evidence to this effect. Thus the estimates on percent dark spots, resistance measurements, and photoelectrochemical measurements indicate the beneficial aspects of a coil over a mesh architecture. The reduction of such recombination centers in a coil is the reason for the higher photovoltage and photocurrent. Further the higher photo(electro)catalytic conversion reported in Table 3 is indicative of externally aided improved electron transport. The greater degradation with coil can be attributed to the availability of more photogenerated holes.

4.4. Adjustable spacing and curvature

Wires of Ti can be coiled around supports to alter the coil diameter (ϕ) and/or successive coil spacing (s) as shown in Fig. 8. Examples of some configuration include circular, elliptical, and hair pin arrangements of each coil turn. This option allows for maximizing light–T-NT interaction without compromising on any of the benefits discussed in the earlier two points. An immediate advantage of this adjustable spacing and curvature is the possibility to control photodegradation mechanism and the composition of the byproduct(s) in a flow through system, particularly in the aqueous phase. Alternately, with the coil geometry one can also consider placing coils of different diameters in a concentric arrangement with each turns offset in such a way so as to maximize light collection without the presence of any nodes.

5. Conclusions

In conclusion, the physical features (length and diameter) and photo(electro)catalytic properties of T-NT formed on two specific non-planar geometries (mesh and coil) have been compared. Under the experimental conditions reported in this work, T-NT on the coil architecture shows a 30% improvement in the photodegradation of a textile dye methyl orange compared to T-NT on mesh. Gaseous-phase photodegradation using T-NT formed on coils shows ~50% conversion with a test compound. Photoelectrochemical measurements (I–t and V_{oc} studies) indicate that separation of photoinduced charges is best in T-NT on coils than T-NT on mesh or foil. Further, T-NT grown on the coil architecture offers advantages such as significantly low dark spots, highly reduced recombination centers, and adjustable spacing and dimensions for tuning photocatalytic activity. The coil geometry may also be useful in other unrelated applications such as a support for catalysts in high temperature catalysis.

Acknowledgements

RSV would like to thank Dr. Mo Ahmedian for assisting with SEM imaging and Dr. Bratindranath Mukerjee with the diffuse reflectance measurements. The funding from DOE through grant DE-EE0000272 is also appreciated.

Appendix A. Supplementary data

Supplementary data associated with this article can be found, in the online version, at doi:10.1016/j.apcatb.2011.08.005.

References

[1] K. Vinodgopal, D.E. Wynkoop, P.V. Kamat, Environ. Sci. Technol. 30 (1996) 1660–1666.
[2] M.R. Hoffmann, S.T. Martin, W.Y. Choi, D.W. Bahnemann, Chem. Rev. 95 (1995) 69–96.
[3] A. Fujishima, X. Zhang, D.A. Tryk, Surf. Sci. Rep. 63 (2008) 515–582.
[4] K. Mehrotra, G.S. Yablonsky, A.K. Ray, Ind. Eng. Chem. Res. 42 (2003) 2273–2281.
[5] V. Subramanian, P.V. Kamat, E.E. Wolf, Ind. Eng. Chem. Res. 42 (2003) 2131–2138.
[6] J.S. Lee, W.Y. Choi, J. Phys. Chem. B 109 (2005) 7399–7406.
[7] A.G. Agrios, P. Pichat, J. Appl. Electrochem. 35 (2005) 655–663.
[8] K. Demeestere, J. Dewulf, H.V. Langenhove, Crit. Rev. Environ. Sci. Technol. 37 (2007) 489–538.
[9] D.W. Bahnemann, M. Hilgendorff, R. Memming, J. Phys. Chem. B 101 (1997) 4265–4275.
[10] R.R. Bacsa, J. Kiwi, Appl. Catal. B: Environ. 16 (1998) 19–29.
[11] M. Toyoda, Y. Nanbu, Y. Nakazawa, M. Hirano, M. Inagaki, Appl. Catal. B: Environ. 49 (2004) 227–232.
[12] S.B. Kim, S.C. Hong, Appl. Catal. B: Environ. 35 (2002) 305–315.
[13] Y. Zhiyong, H. Keppner, D. Laub, E. Mielczarski, J. Mielczarski, A. Renken, J. Kiwi, Appl. Catal. B: Environ. 79 (2008) 63–71.
[14] N. Serpone, I. Texier, A.V. Emeline, P. Pichat, H. Hidaka, J. Zhao, J. Photochem. Photobiol. A: Chem. 136 (2000) 145–155.
[15] R. Beranek, H. Tsuchiya, T. Sugishima, J.M. Macak, L. Taveira, S. Fujimoto, H. Kisch, P. Schmuki, Appl. Phys. Lett. 87 (2005), 243114_243111-243113.
[16] W.D. Wang, P. Serp, P. Kalck, J.L. Faria, Appl. Catal. B: Environ. 56 (2005) 305–312.
[17] Y. Sohn, Y. Smith, M. Misra, V. Subramanian, Appl. Catal. B: Environ. 84 (2008) 372–378.
[18] A. Kongkanand, K. Tvrdy, K. Takechi, M. Kuno, P.V. Kamat, J. Am. Chem. Soc. 130 (2008) 4007–4015.
[19] C.J. Lin, Y.H. Yu, Y.H. Liou, Appl. Catal. B: Environ. 93 (2009) 119–225.
[20] H.F. Zhuang, C.J. Lin, Y.K. Lai, L. Sun, J. Li, Environ. Sci. Technol. 41 (2007) 4735–4740.
[21] J.M. Macak, H. Tsuchiya, P. Schmuki, Angew. Chem. Int. Ed. 44 (2005) 2100–2102.
[22] Y.K. Lai, L. Sun, Y.C. Chen, H.F. Zhuang, C.J. Lin, J.W. Chin, J. Electrochem. Soc. 153 (2006) D123–D127.
[23] G.K. Mor, O.K. Varghese, M. Paulose, K. Shankar, C.A. Grimes, Sol. Energy Mater. Sol. Cells 90 (2006) 2011–2075.
[24] K. Shankar, J. Bandara, M. Paulose, H. Wietasch, O.K. Varghese, G.K. Mor, T.J. LaTempa, M. Thelakkat, C.A. Grimes, Nano Lett. 8 (2008) 1654–1659.
[25] G.K. Mor, O.K. Varghese, M. Paulose, C.A. Grimes, Adv. Funct. Mater. 15 (2005) 1291–1296.
[26] Z.Y. Liu, V. Subramania, M. Misra, J. Phys. Chem. C 113 (2009) 14028–14033.
[27] Z. Liu, M. Misra, ACS Nano 4 (2010) 2196–2200.
[28] A. Kar, Y.R. Smith, V. Subramanian, Environ. Sci. Technol. 43 (2009) 3260–3265.
[29] Z.H. Zhang, Y. Yuan, L.H. Liang, Y.J. Fang, Y.X. Cheng, H.C. Ding, G.Y. Shi, L.T. Jin, Ultrason. Sonochem. 15 (2008) 370–375.
[30] M. Tian, G. Wu, B. Adams, J. Wen, A. Chen, J. Phys. Chem. C 112 (2008) 825–831.
[31] Z.B. Wu, S. Guo, H.Q. Wang, Y. Liu, Electrochem. Commun. 11 (2009) 1692–1695.
[32] Y.Y. Huang, F.Q. Sun, H.J. Wang, Y. He, L.S. Li, Z.X. Huang, Q.S. Wu, J.C. Yu, J. Mater. Chem. 19 (2009) 6901–6906.
[33] V.K. Mahajan, M. Misra, K.S. Raja, S.K. Mohapatra, J. Phys. D: Appl. Phys. 41 (2008).
[34] K.S. Raja, T. Gandhi, M. Misra, Electrochem. Commun. 9 (2007) 1069–1076.
[35] V. Subramanian, R.K. Roeder, E.E. Wolf, Ind. Eng. Chem. Res. 45 (2006) 2187–2193.
[36] K.S. Raja, M. Misra, K. Paramguru, Electrochim. Acta 51 (2005) 154–165.
[37] V. Subramanian, Interface 16 (2007) 32–36.
[38] S. Mondal, Environ. Eng. Sci. 25 (2008) 383–396.
[39] C. Hachem, F. Bocquillon, O. Zahraa, M. Bouchy, Dyes Pigments 49 (2001) 117–125.
[40] A. Fujishima, T.N. Rao, D.A. Tryk, J. Photochem. Photobiol. C 1 (2000) 1–21.
[41] I.N. Chernozemsky, E. Boyland, Iarc Scientific Publications, 1981, pp. 3–12.
[42] I.K. Konstantinou, T.A. Albanis, Appl. Catal. B: Environ. 49 (2004) 1–14.
[43] Z.H. Zhang, Y. Yuan, G.Y. Shi, Y.J. Fang, L.H. Liang, H.C. Ding, L.T. Jin, Environ. Sci. Technol. 41 (2007) 6259–6263.
[44] X. Jiang, T. Wang, Environ. Sci. Technol. 41 (2007) 4441–4446.
[45] I.M. Arabatzis, T. Stergiopoulos, D. Andreeva, S. Kitova, S.G. Neophytides, P. Falaras, J. Catal. 220 (2003) 127–135.
[46] N.Z. Bao, X. Feng, Z.H. Yang, L.M. Shen, X.H. Lu, Environ. Sci. Technol. 38 (2004) 2729–2736.
[47] C. Baiocchi, M.C. Brussino, E. Pramauro, A.B. Prevot, L. Palmisano, G. Marci, Int. J. Mass Spectrom. 214 (2002) 247–256.
[48] Y. Smith, A. Kar, V.R. Subramanian, Ind. Eng. Chem. Res. 48 (2009) 10268–10276.
[49] H.S. Fogler, M.N. Gurmen, Elements of Chemical Reaction Engineering, Prentice Hall, 2006.
[50] F.G.B.G.J. van Rooy, J.M. Rooyackers, M. Prokop, R. Houba, L.A.M. Smit, D.J.J. Heederik, Am. J. Respir. Crit. Care Med. 178 (2008) 313–314.
[51] F.G.B.G.J. van Rooy, L.A.M. Smit, R. Houba, V.A.C. Zaat, J.M. Rooyackers, D.J.J. Heederik, Occup. Environ. Med. 66 (2009) 105–110.
[52] V. Hoang, P. Pichat, H. Courbon, J. Disdier, 4th Intl. Conf. Characterization Ctrl Emissions Odors VOCs, Montreal, Canada, 1997, pp. 468–489.
[53] J. Nelson, Phys. Rev. B 59 (1999) 15374–15380.